

# Equation of state of neutron star matter and its warm extension with an interacting hadron resonance gas

Yuki Fujimoto<sup>a</sup>, Kenji Fukushima<sup>a</sup>, Yoshimasa Hidaka<sup>b,c,d</sup>, Atsuki Hiraguchi<sup>e,f</sup>, Kei Iida<sup>f</sup>

<sup>a</sup>Department of Physics, The University of Tokyo, 7-3-1 Hongo, Bunkyo-ku, Tokyo 113-0033, Japan

<sup>b</sup>Institute of Particle and Nuclear Studies, KEK, 1-1 Oho, Tsukuba, Ibaraki 305-0801 Japan

<sup>c</sup>Graduate University for Advanced Studies (Sokendai), Tsukuba 305-0801, Japan

<sup>d</sup>RIKEN iTHEMS, RIKEN, 2-1 Hirosawa, Wako, Saitama 351-0198, Japan

<sup>e</sup>Institute of Physics, National Yang Ming Chiao Tung University, Hsinchu 30010, Taiwan

<sup>f</sup>Department of Mathematics and Physics, Kochi University, Kochi 780-8520, Japan

## Abstract

We propose an interpolating equation of state that satisfies phenomenologically established boundary conditions in two extreme regimes at high temperature and low baryon density and at low temperature and high baryon density. We confirm that the hadron resonance gas model with the Carnahan-Starling excluded volume effect can reasonably fit the empirical equation of state at high density up to several times the normal nuclear density. We identify the onsets of strange particles and quantify the strangeness contents in dense matter. We finally discuss the finite temperature effects and estimate the thermal index  $\Gamma_{\text{th}}$  as a function of the baryon density, which should be a crucial input for the core-collapse supernova and the binary neutron star merger simulations.

## 1. Introduction

Strongly interacting matter has been investigated well in two extremes of the temperature  $T$  and baryochemical potential  $\mu_B$ . The heavy-ion collision experiments realize matter at high- $T$  and low- $\mu_B$ , which can also be studied by the Monte-Carlo simulation of quantum chromodynamics (QCD) on the lattice [1, 2]. Another extreme matter at low- $T$  and high- $\mu_B$  is found in cores of neutron stars, for which the Monte-Carlo lattice-QCD simulation is of no use due to the notorious sign problem.

Confronting the lattice-QCD thermodynamics, the hadron resonance gas (HRG) model has become a common tool to approximate the equation of state (EoS) below the critical temperature  $T_c \sim 150$  MeV (see, e.g., Ref. [3] for a recent review). The HRG model is a parameter-free description of thermal properties with experimentally observed particle and resonance spectra. In the HRG model, nonperturbative hadronic interactions are assumed to be dominated by poles and branch cuts corresponding to resonances [4]. The ideal HRG (IHRG) model consists of noninteracting hadrons and resonances, and yet, its validity has been endorsed by the successful thermal fit of particle abundances in heavy-ion collision experiments. The IHRG EoS is recently extended to the terrain of finite baryochemical potential in a region of  $\mu_B/3 \lesssim T$  [5], guided

by the conserved charge susceptibilities from lattice-QCD calculations [6–8]. This region may include a possibility of Quarkyonic matter [9–13] and the associated triple-point structure in the QCD phase diagram [14]. Furthermore, owing to its parameter-free nature, it can also be applied to a wide variety of problems such as a reference for baryon number fluctuations [15], a shift of the chemical freeze-out due to the inverse magnetic catalysis [16], and the rotational effect on the deconfinement temperature [17], to mention a few.

Thermodynamic quantities from the IHRG model, however, blow up above  $T_c$ . We expect that the validity region of the HRG model could be extended to higher temperature by introducing the *interaction effect*. The excluded volume (EV) effect is the simplest way to implement the interacting HRG and the formulation was given in Ref. [18]; the short-range repulsive interaction was modeled via a hard-core correction following the thermodynamically consistent way as developed in Ref. [19] (see also Ref. [20]). By supplementing the repulsive interaction with an additional attractive interaction, the interacting HRG model amounts to the van der Waals (VDW) EoS [21, 22] (see also Ref. [23] and references therein).

Up to here, we have reviewed the interacting HRG model in the context of high- $T$  and low- $\mu_B$  studies. Then, it is a natural anticipation that the same machinery of the interacting HRG model can also work at low- $T$  for astrophysical applications; interestingly enough, this idea of applying the HRG description for neutron stars can be traced back to the pioneering work by Hagedorn [24] more

Email addresses: fujimoto@nt.phys.s.u-tokyo.ac.jp

(Yuki Fujimoto), fuku@nt.phys.s.u-tokyo.ac.jp

(Kenji Fukushima), hidaka@post.kek.jp (Yoshimasa Hidaka),

a.hiraguchi@nycu.edu.tw (Atsuki Hiraguchi), iida@kochi-u.ac.jp

(Kei Iida)

than half a century ago even before the discovery of pulsars. One might think that this anticipation is immediately falsified by the nuclear liquid-gas phase transition of first order in the low- $T$  and high- $\mu_B$  region. Although the IHRG model is unable to describe the first-order phase transition, the interacting VDW-HRG model can properly account for the liquid-gas phase transition as studied in Refs. [21, 25].

In the present work, we will look into the EoS from the VDW-HRG model by making a quantitative comparison with the Chiral Effective Field Theory ( $\chi$ EFT). We will show that the hard-core EV effect violates the causality, but the VDW-HRG model with refined repulsive interaction works quite well at low  $T$  and high  $\mu_B$ . The modified repulsive interaction is incorporated à la Carnahan-Starling (CS) [26]. The CS excluded volume has been adopted in the hadron physics [27–29], and astrophysics [30, 31]. Within the HRG model with the CS-type EV, i.e., the CS-HRG model, we will construct the EoS,  $p(n_B)$  (the pressure vs. the baryon number density), for dense and warm matter at  $T < 60$  MeV. Even though the parameters in the CS-HRG model are fixed by the  $\chi$ EFT, the CS-HRG can provide us with useful insights. One example is that we can diagnose the strangeness contents in dense matter hadron by hadron. Another useful application is the finite- $T$  extension of the EoS; in many simulations of binary neutron star mergers the thermal component of the EoS is treated as an ideal gas for convenience [32, 33], and there is a recent discussion in the astrophysical context [34] that thermal pions could be important.

At the conceptual level, the interacting HRG model embodies the idea of Quarkyonic matter that claims continuous duality between baryonic and quark matter (see, however, Ref. [35] for the earlier analysis based on the VDW model indicating the large- $N_c$  transition between  $N_c = 3$  and  $N_c \rightarrow \infty$ ). The idea is consonant to the crossover EoS construction based on quark-hadron continuity [36–38]. There are theoretical attempts to build a Quarkyonic model [39–46], and as argued in a quantum percolation picture [47] quark degrees of freedom emerge from interactions. In this sense, the interacting HRG model could be regarded as a concrete modeling that exhibits the quark-hadron duality from the hadronic side. This theoretical argument also justifies the extended validity of the interacting hadronic model for high- $T$  and/or high- $\mu_B$  matter in which quark degrees of freedom could be mixed together.

We note that, throughout this work, we use natural units;  $c = \hbar = k_B = 1$ .

## 2. Interacting hadron resonance gas model

The HRG encompasses the numerous contributions from experimentally measured states of hadrons and resonances. The total thermodynamic quantities, such as the

pressure, can be decomposed into three pieces:

$$p(T, \boldsymbol{\mu}) = p_M(T, \boldsymbol{\mu}) + p_B(T, \boldsymbol{\mu}) + p_{\bar{B}}(T, \boldsymbol{\mu}), \quad (1)$$

where  $M$ ,  $B$ , and  $\bar{B}$  denote contributions from mesons, baryons, and anti-baryons, respectively, and  $\boldsymbol{\mu} = (\mu_B, \mu_Q, \mu_S)$  are the chemical potentials conjugate to the net baryon number  $B$ , the electric charge  $Q$ , and the strangeness  $S$ . We here limit ourselves to  $B = 1$  baryons and  $B = -1$  anti-baryons, and we discard composite baryons with  $B > 1$  such as the deuteron, light nuclei, hypernuclei, etc.; the deuteron, for example becomes unbound in neutron-rich matter. Moreover, since matter itself is a gigantic nucleus (if it is self-bound), light cluster contributions may lead to double-counting problems. For our HRG model in this work, we have adopted the particle data group list of particles and resonances (where the resonances are handled in the zero-width approximation; see Ref. [48] for a refined  $S$ -matrix treatment of resonances) contained in the THERMUS-V3.0 package [49].

### 2.1. Ideal hadron resonance gas (IHRG)

In the IHRG model, each particle is treated as the Bose/Fermi ideal (i.e., non-interacting) gas. In this model, the mesonic, the baryonic, and the anti-baryonic contributions in Eq. (1) are given by

$$p_{M/B/\bar{B}}(T, \boldsymbol{\mu}) = \sum_{i \in M/B/\bar{B}} p_i^{\text{id}}(T, \mu_i), \quad (2)$$

where the pressure function  $p_i^{\text{id}}$  in the grand canonical ensemble is

$$p_i^{\text{id}}(T, \mu_i) = \pm \frac{g_i T}{2\pi^2} \int_0^\infty k^2 dk \ln \left[ 1 \pm e^{-(E_i - \mu_i)/T} \right]. \quad (3)$$

We note that the overall  $+$  ( $-$ ) sign corresponds to the fermion (boson). The energy dispersion is  $E_i = \sqrt{k^2 + m_i^2}$  with the spin degeneracy factor,  $g_i = 2s_i + 1$ , and the chemical potential,  $\mu_i = B_i \mu_B + Q_i \mu_Q + S_i \mu_S$ , of the particle species  $i$ .

The other thermodynamic quantities such as the number density  $n_i$  and the energy density  $\varepsilon_i$  can also be derived accordingly as

$$n_i^{\text{id}}(T, \mu_i) = \frac{g_i}{2\pi^2} \int_0^\infty \frac{k^2 dk}{e^{(E_i - \mu_i)/T} \pm 1}, \quad (4)$$

$$\varepsilon_i^{\text{id}}(T, \mu_i) = \frac{g_i}{2\pi^2} \int_0^\infty \frac{k^2 dk}{e^{(E_i - \mu_i)/T} \pm 1} E_i. \quad (5)$$

For cold matter at  $T = 0$  we can analytically carry out the fermion integrals (and mesons are irrelevant) to find the pressure,  $p_i^{\text{id}}(\mu_i) = \frac{g_i}{24\pi^2} \left[ \mu_i k_{F,i} (\mu_i^2 - \frac{5}{2} m_i^2) + \frac{3}{2} m_i^4 \ln \left( \frac{k_{F,i} + \mu_i}{m_i} \right) \right]$ , and the number and the energy densities are  $n_i^{\text{id}}(\mu_i) = \frac{g_i}{6\pi^2} k_{F,i}^3$  and  $\varepsilon_i^{\text{id}}(\mu_i) = \frac{g_i}{16\pi^2} \left[ \mu_i k_{F,i} (2\mu_i^2 - m_i^2) - m_i^4 \ln \left( \frac{k_{F,i} + \mu_i}{m_i} \right) \right]$ , with the Fermi momentum being  $k_{F,i} = \sqrt{\mu_i^2 - m_i^2}$ .

## 2.2. Van der Waals hadron resonance gas (VDW-HRG)

In this work, we incorporate the interaction effect based on the VDW construction, which comprises the repulsive interaction by the EV effect and the attractive interaction. The VDW EoS was originally formulated in classical systems in the canonical ensemble with the fixed number of particles, and thus the following two extensions were necessary: the reformulation in the grand canonical ensemble was given in Ref. [25], and the quantum statistics was taken into account in Refs. [50, 51]. Hereafter, we will employ the formulation in Ref. [52]. At this point, we shall make a comment on the interactions. We will consider the interaction effect only in the  $B$  sector. At zero and low temperatures, the  $\bar{B}$  sector is simply negligible. The reason why we neglect the interaction in the  $M$  sector is that mesons are only weakly interacting in the limit of large colors. Indeed, the substantial mesonic EV effect leads to the discrepancy between the EV-HRG and the lattice-QCD data due to too strong suppression of thermodynamic quantities, which was already implied in Figure 4 of Ref. [18].

To introduce the repulsive interaction through the EV effect, we replace the volume  $V$  in the partition function by  $f(\eta)V$  with  $\eta$  being the packing fraction<sup>1</sup>. The function  $f(\eta) \in (0, 1]$  measures the volume fraction in which particles with hard sphere can move around. The concrete expression of  $f(\eta)$  will be given soon in Eqs. (11), and (12). The packing fraction,  $\eta$ , is defined as  $\eta = bn/4$  where  $b = \frac{1}{2} \times \frac{4\pi}{3} (2R)^3$  is the eigenvolume of a hadron with a hard-sphere radius  $R$ . We note that the inter-particle distance cannot be less than  $2R$  and the EV per a particle pair is  $\frac{4\pi}{3} (2R)^3$ , and  $1/2$  is further needed for one particle.

The VDW-HRG model in the  $B$  sector can be obtained by the following implicit equation:

$$n_B(T, \boldsymbol{\mu}) = f(\eta_B) \sum_{i \in B} n_i^{\text{id}}(T, \hat{\mu}_i), \quad (6)$$

where the shifted chemical potential  $\hat{\mu}_i$  is

$$\hat{\mu}_i = \mu_i + \Delta\mu_B, \quad (7)$$

$$\Delta\mu_B = \frac{b_B}{4} f'(\eta_B) \sum_{i \in B} p_i^{\text{id}}(T, \hat{\mu}_i) + 2an_B. \quad (8)$$

The last term  $\propto a$  represents the attractive interaction effect. With the solution from Eqs. (6)-(8), we can compute the pressure and the energy as follows:

$$p_B(T, \boldsymbol{\mu}) = [f(\eta_B) - \eta_B f'(\eta_B)] \sum_{i \in B} p_i^{\text{id}}(T, \hat{\mu}_i) - an_B^2, \quad (9)$$

$$\varepsilon_B(T, \boldsymbol{\mu}) = f(\eta_B) \sum_{i \in B} \varepsilon_i^{\text{id}}(T, \hat{\mu}_i) - an_B^2. \quad (10)$$

<sup>1</sup>Strictly speaking, the EV effect has to be introduced through the canonical partition function as formulated originally.

For the conventional VDW model, the standard choice of  $f(\eta)$  is

$$f_{\text{VDW}}(\eta) = 1 - 4\eta. \quad (11)$$

By definition the range of  $f_{\text{VDW}}(\eta)$  must be limited within  $0 < f_{\text{VDW}}(\eta) \leq 1$ , where  $f_{\text{VDW}} = 1$  refers to the no EV limit and  $f_{\text{VDW}} = 0$  corresponds to the maximal packing. When the maximal packing is reached at  $\eta = 1/4$ , the thermodynamic quantities become singular. Singularity in the thermodynamic quantities at the maximal packing leads to the acausal behavior in the speed of sound  $c_s > 1$ , where the speed of sound is defined as  $c_s^2 \equiv \partial p / \partial \varepsilon$ . In the neutron star environment, using the hard-sphere radius  $R_B = 0.511$  fm (which will be determined in Sec. 4.1), we have a rough estimate for the maximal packing density as to  $n_B \simeq 2.8n_0$  and the density at which the superluminal speed of sound ( $c_s > 1$ ) is reached as to  $n_B \simeq 2.2n_0$ ;  $n_0 = 0.16$  fm<sup>-3</sup> is the normal nuclear density. These values are lower than the density in central cores of typical-mass neutron stars, and the above simple choice (11) is obviously inappropriate.

## 2.3. Carnahan-Starling (CS) refinement of the excluded volume term

In the VDW-type EV treatment, the interaction sphere is too rigid and the maximal packing occurs at unphysically low density. It would be sensible to smear the interaction clouds so that the EV effects can mildly set in. For the astrophysical application, therefore, we should improve the function (11) and a promising candidate is the Carnahan-Starling (CS)-type EV [26].

For the CS-HRG model [52], the choice of  $f(\eta)$  is

$$f_{\text{CS}}(\eta) = \exp \left[ -\frac{(4 - 3\eta)\eta}{(1 - \eta)^2} \right]. \quad (12)$$

When  $\eta \ll 1$ , we can easily confirm that  $f_{\text{CS}}(\eta) \approx 1 - 4\eta = f_{\text{VDW}}(\eta)$  up to the linear order in  $\eta$ . Here again, the range of  $f_{\text{CS}}$  must be limited within  $0 < f_{\text{CS}} \leq 1$ . The maximal packing occurs at  $\eta = 1$ . The corresponding density,  $n_B = 4\eta/b = 3/(4\pi R_B^3)$ , then reaches  $n_B = 11.2n_0$  with  $R_B = 0.511$  fm. Because of a longer tail up to  $\eta \sim 1/2$  in Eq. (12) as compared to a sharp drop at  $\eta = 1/4$  in Eq. (11), the maximal packing density in the CS-type EV is about four times larger than that of the VDW-type EV, which extends the validity range. This is a naïve estimate, and the serious calculation concerning the causality gives a rather smaller value of the limiting density, i.e.,  $n_B \simeq 3.7n_0$  for  $R_B = 0.511$  fm.

## 2.4. Need for the attractive interaction

In the spirit of the HRG model, the attractive interaction leading to the resonance formation is implicitly incorporated through added resonances; however, not all the attractive interactions are taken into account by resonances. The nuclear force has attractive regions, which are dominated by one-pion exchange, as well as repulsive regions by

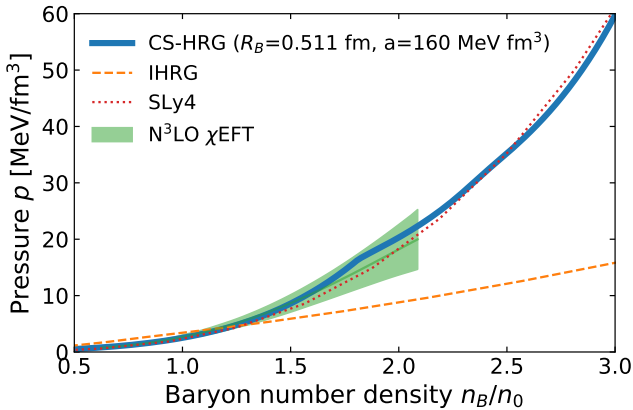


Figure 1: EoS calculated from the CS-HRG model at  $T = 0$ . The IHRG results and the phenomenological nuclear EoS (SLy4 [54]), together with the  $N^3\text{LO } \chi\text{EFT}$  EoS [55, 56] (to which our parameters are fitted) are shown.

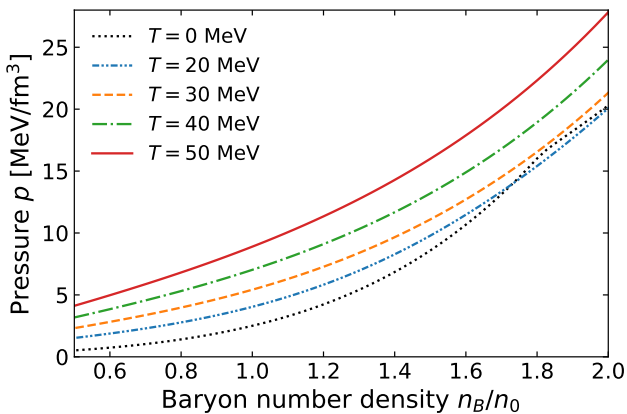


Figure 2: EoS calculated from the CS-HRG model at finite  $T$ . The  $T = 0$  results are the same as shown in Fig. 1 but the scale is magnified.

the exchange of heavy mesons and multi-pions, as seen also in the first-principles lattice-QCD calculation [53]. The VDW model can deal with such characteristics of the nuclear force; the EV effect captures the repulsive core nature at short range, while the intermediate and long-range parts are reasonably captured by resonances and the attractive interaction term in the VDW model.

One might wonder how that the attractive term  $\propto a$  affects physical observables. Only to avoid singular behavior of thermodynamic quantities, the minimal model with either VDW- or CS-type EV would be enough. We would, however, stress that the attractive term is indispensable for quantitative analysis. We will come back to this point when we discuss the  $M$ - $R$  relation using the EoS from the CS-HRG model later.

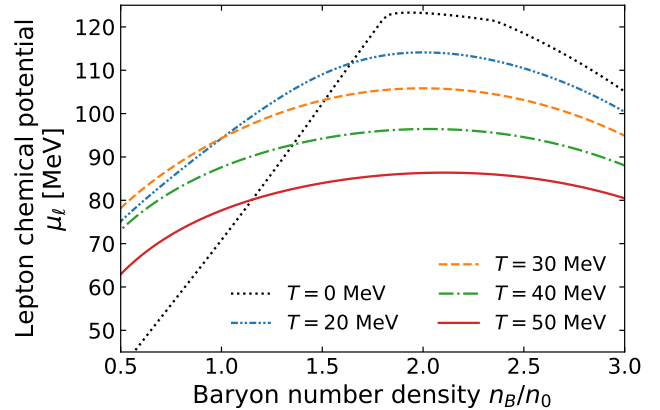


Figure 3: Lepton chemical potential  $\mu_\ell = -\mu_Q$  obtained by solving the electric charge neutrality and the  $\beta$ -equilibrium conditions.

### 3. EoS construction

We are ready to construct the EoS for neutron stars at  $T = 0$  as well as for compact-binary mergers and supernovae at  $T > 0$ . Under these circumstances, the system is  $\beta$ -equilibrated via the weak processes such as

$$n \rightarrow p + \ell + \bar{\nu}_\ell, \quad p + \ell \rightarrow n + \nu_\ell, \quad (13)$$

$$\Sigma^- \rightarrow n + \ell + \bar{\nu}_\ell, \quad n + \ell \rightarrow \Sigma^- + \nu_\ell, \quad (14)$$

and neutral in the electric charge. These conditions of  $\beta$ -equilibrium and electric charge neutrality amount to setting the values of the chemical potentials,  $\mu_Q$  and  $\mu_S$ .

Owing to large asymmetry of baryons and anti-baryons at high  $\mu_B$ , we can safely neglect the anti-baryonic contribution to the EoS, and we can also drop the mesonic contribution at  $T = 0$ . The meson condensation would cause subtlety; in particular, negatively charged pions would form a condensate when  $\mu_\ell > m_{\pi^-}$ , where  $\mu_\ell$  is the leptochemical potential and  $m_\pi = 140$  MeV is the pion mass. We assume no condensate and this will be justified self-consistently as shown in Fig. 3. The values of  $\mu_\ell$  at various temperatures in Fig. 3 do not exceed  $m_\pi$ .

We impose the following conditions on  $\mu_Q$  and  $\mu_S$ :

$$n_Q(T, \boldsymbol{\mu}) - n_\ell(T, \mu_\ell) = 0, \quad (15)$$

$$\mu_S = 0, \quad (16)$$

where  $n_Q$  is the electric charge density in the interacting HRG model, whose expression is given by

$$n_Q(T, \boldsymbol{\mu}) = f(\eta_B) \sum_{i \in B} Q_i n_i^{\text{id}}(T, \mu_B + \Delta\mu_B + Q_i \mu_Q) + \sum_{i \in M} Q_i n_i^{\text{id}}(T, Q_i \mu_Q). \quad (17)$$

For the expression of the lepton density,  $n_\ell$ , we substitute the electron mass,  $m_e = 0.511$  MeV, and the muon mass,

$m_\mu = 106 \text{ MeV}$  for the mass in the free particle expression (4):

$$n_\ell(T, \mu_\ell) = n_{i=e}^{\text{id}}(T, \mu_\ell; m_e) + n_{i=\mu}^{\text{id}}(T, \mu_\ell; m_\mu). \quad (18)$$

We neglected the neutrino contribution by assuming that neutrinos quickly escape in neutron star systems both for  $T = 0$  and  $T > 0$ . Now we can solve these conditions to find

$$\mu_Q + \mu_\ell = 0, \quad \mu_S = 0. \quad (19)$$

For the actual procedures, we fix the value of  $n_B$ , and solve Eqs. (6)-(8), (15), and (16) in terms of three variables,  $\mu_B$ ,  $\mu_Q (= -\mu_\ell)$ , and  $\Delta\mu_B$ . Once three variables are obtained, we can compute the thermodynamic quantities correspondingly. We note in passing that  $\mu_B$  and  $\Delta\mu_B$  always appear in the combination of  $\hat{\mu}_B \equiv \mu_B + \Delta\mu_B$ , so that we can separately treat Eq. (8) and solve two coupled equations to determine  $\hat{\mu}_B$  and  $\mu_Q$ .

With bearing the application to neutron stars in mind, we calculate the EoS at  $T = 0$  following the procedures outlined above. We plot our main results for the EoS from the CS-HRG model in Fig. 1. The two parameters,  $R_B$  and  $a$ , are fitted to reproduce the N<sup>3</sup>LO  $\chi$ EFT EoS, which is taken from Ref. [55] based on the pure neutron and symmetric nuclear matter calculations [56]. It is evident from the comparison between our results (by the thick curve) and the IHRG results (by the dashed curve) that the interaction is crucial for neutron star matter. We also observe that our fitted EoS stays close to the phenomenological nuclear EoS, for which we choose SLy4 [54]. It should be noted that the VDW-HRG model with  $f_{\text{VDW}}(\eta)$  in Eq. (11) can by no means fit the N<sup>3</sup>LO  $\chi$ EFT nor the SLy4 EoS at all. In Fig. 1 there appears a bump around the  $n_B = 1.8n_0$ ; it is related to the onset of hyperons as discussed later in Fig. 5. Here, too rapid stiffening is tamed by softening induced by the appearance of hyperons.

The interacting HRG model has originally been used in the finite- $T$  circumstances, so it should be a reasonable setup for generalizing the EoS construction to the finite- $T$  case. In this way, the finite- $T$  EoS has been obtained from the CS-HRG model and we plot the results at  $T = 0, 20, 30, 40,$  and  $50 \text{ MeV}$  in Fig. 2. Overall, the pressure becomes higher with increasing  $T$  as expected, but we find an exception; the EoS at  $T = 20 \text{ MeV}$  goes below the  $T = 0$  EoS around  $n_B \simeq 1.8n_0$ . We can understand this as follows. At  $T = 0$  new particles cannot appear until the density exceeds the mass threshold. Below the onset density, the EoS becomes stiffer as the density rises up. On the other hand, at finite  $T$ , the EoS can accommodate any massive particles according to the thermal weights, which makes a qualitative difference from the  $T = 0$  EoS and explains the change of the ordering around  $n_B \simeq 1.8n_0$ .

Finally, we show the leptochemical potential  $\mu_\ell$  in Fig. 3. As we already mentioned before,  $\mu_\ell$  never exceeds the pion mass for any temperature and density. This self-consistently justifies our assumption of no meson condensate.

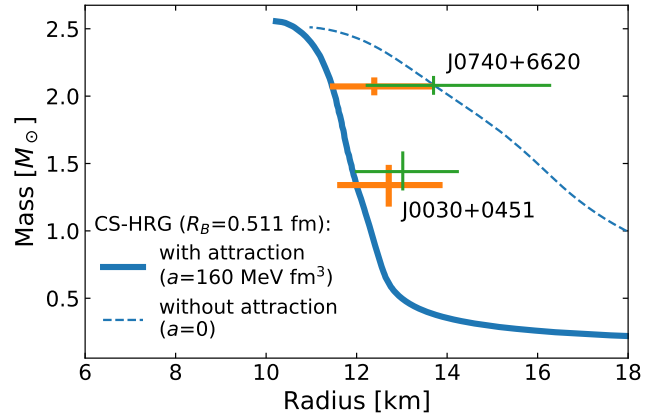


Figure 4:  $M$ - $R$  relation corresponding to the EoS in Fig. 1. The thick (dashed) curve represents the result with (without) the attractive interaction. The radius constraints from the NICER collaboration are shown: (J0030+0451 at  $M = 1.4 M_\odot$ ) Ref. [57] and Ref. [58] conclude a smaller (84 % CL) and a larger (68 % CL) radius, respectively. (J0740+6620 at  $M = 2 M_\odot$ ) Ref. [59] and Ref. [60] conclude a smaller (84 % CL) and a larger (68 % CL) radius, respectively.

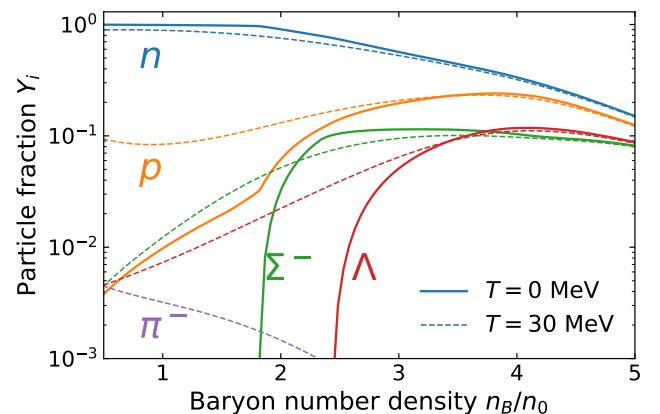


Figure 5: Particle fraction  $Y_i = n_i/n_B$  corresponding to the EoS in Fig. 1. The finite- $T$  results are overlaid by dotted curves.

## 4. Astrophysical applications

We will showcase the numerical results for the EoS and the phenomenological implications at  $T = 0$  and finite  $T$  in order.

### 4.1. Neutron star matter and structure at $T = 0$

With the EoS from the CS-HRG model, we calculate the mass-radius ( $M$ - $R$ ) relation by solving the Tolman-Oppenheimer-Volkoff (TOV) equation. As shown in Fig. 4, our EoS incidentally matches with the phenomenologically accepted EoSs such as SLy4, even in the crust region of neutron stars, and so we use our EoS down to the surface of the star when solving the TOV equation; see Ref. [61]. We compare the cases with/without the attractive interaction. If we turn off the attractive interaction at  $a = 0$ , the radius at  $M = 1.4 M_\odot$  is too large and out of the NICER

observation as seen in Fig. 4. Usually, the lower density part of the EoS is responsible for the radius of stars, and a larger radius is favored for a stiffer EoS at low density. This tendency can be confirmed in Fig. 1; the IHRG EoS is constructed without the attractive interaction, and the lower density part ( $n_B/n_0 \lesssim 1$ ) from the IHRG model exceeds that from the CS-HRG model. This behavior is consistent with such an interpretation that the EoS without attractive interaction gives too stiff EoS at low density and leads to a too large radius.

As mentioned earlier, for  $R_B = 0.511$  fm, the maximum packing density, above which the model breaks down, is  $n_B = 11.2 n_0$  for the CS-HRG model. On the  $M$ - $R$  relation, the maximum mass of  $M = 2.56 M_\odot$  is attained at  $n_B = 9.32 n_0$ , which certainly lies within the validity range of the CS-HRG model. Regarding the maximum mass, some controversies are unavoidable. Combining the GW170817 event with the accompanying electromagnetic observation, the maximum mass could be constrained to be at most  $\lesssim 2.3 M_\odot$  [62–65]. Meanwhile, a compact object with  $\sim 2.6 M_\odot$  has been observed in the GW190814, which may be identified as a massive neutron star. Near the maximum mass region, another subtlety arises from a possible transition to quark matter [66, 67]. It is a nontrivial question where the validity bound of our model should be. If we locate the validity bound at  $n_B \simeq 3.7 n_0$  (see explanations in Sec. 2.3), our model should be very apt up to  $M \simeq 1.5 M_\odot$ .

The HRG model provides us with a convenient picture to probe the particle abundances. In Fig. 5 we show the fraction  $Y_i = n_i/n_B$  of the particle species  $i$ . At small density, the neutron,  $n$ , is dominant with a small fraction of the proton,  $p$ , which slowly increases with increasing density. The onset of the hyperons is observed slightly below  $2 n_0$ . As is consistent with the conventional scenario (see, e.g., Sec. 5 of Ref. [68]),  $\Sigma^-$  is activated first as we increase the density, and then  $\Lambda$  is produced afterwards.

#### 4.2. Thermal index

In the applications for astrophysical phenomena such as supernovae and binary neutron star mergers, the thermal corrections to the EoS are often modeled by an ideal gas approximation [32, 33, 70]. In order to define the thermal part of the EoS, which is parametrized by the thermal index,  $\Gamma_{\text{th}}$ , we introduce the rest-mass density of baryons as  $\rho_B = m_B n_B$  with the nucleon mass,  $m_B = 939$  MeV. We can decompose the energy density  $\varepsilon$  as  $\varepsilon = (1 + e)\rho_B$ , where  $e$  is the specific internal energy. We can add the thermal corrections to the pressure and the energy on top of the  $T = 0$  parts as

$$p = p_{T=0} + p_{\text{th}}, \quad e = e_{T=0} + e_{\text{th}}. \quad (20)$$

In the simulations of neutron star mergers, the cold ( $T = 0$ ) component is used before shock heating associated with the stellar collision sets in. The relation between the thermal pressure and the energy should be supplemented with

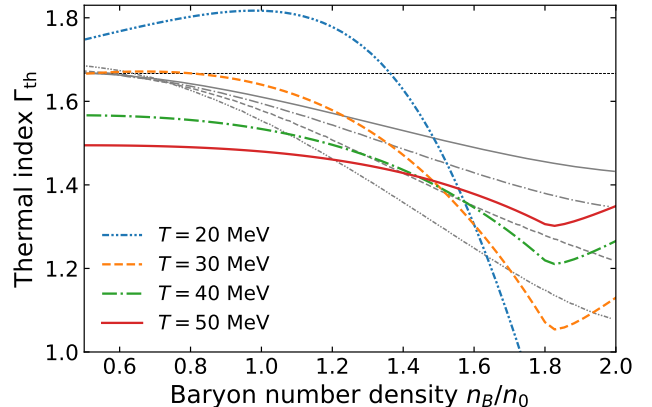


Figure 6: Thermal index  $\Gamma_{\text{th}}$  corresponding to the EoS shown in Fig. 2. For reference, the *ab initio* calculations for pure neutron matter [69] are overlaid in the grey color with the same line style as our results. The canonical value of the adiabatic index for non-relativistic ideal gas,  $\Gamma = 5/3$ , is shown by a horizontal line.

the additional constraint, that is commonly parametrized by

$$p_{\text{th}} = (\Gamma_{\text{th}} - 1)\rho_B e_{\text{th}}. \quad (21)$$

In the phenomenological studies,  $\Gamma_{\text{th}}$  is a free parameter. It is customary to choose  $\Gamma_{\text{th}}$  around  $\sim 1.7$ . For example,  $\Gamma_{\text{th}} = 1.8$  was adopted in Ref. [71]. If  $\Gamma_{\text{th}}$  is too small (like  $\sim 1.3$ ), the thermal pressure is not large enough to sustain matter, resulting in a rapid proto-neutron star contraction for supernovae, and in a faster collapse of merger remnants to black holes for binary merger. In this way, smaller values of  $\Gamma_{\text{th}}$  may have impact on core-collapse supernova and binary neutron star merger simulations [72]. In contrast, a larger  $\Gamma_{\text{th}}$  (like  $\sim 2.0$ ) would elongate the life-time of the post-merger dynamics. Thus, for reliable theoretical predictions, it is of utmost importance to constrain  $\Gamma_{\text{th}}$ . Moreover, although it is often assumed to be constant,  $\Gamma_{\text{th}}$  may depend on the density and temperature [69].

We can make use of our EoS to infer  $\Gamma_{\text{th}}$ , which can be represented in terms of the thermodynamic quantities as

$$\Gamma_{\text{th}} = 1 + \frac{p_{\text{th}}}{e_{\text{th}}\rho_B} = 1 + \frac{p_{\text{th}}}{\varepsilon_{\text{th}}}. \quad (22)$$

Here,  $\varepsilon_{\text{th}} = \rho_B e_{\text{th}}$  is the thermal part of the energy density. In Fig. 6, we show our estimate for the thermal index,  $\Gamma_{\text{th}}$ , as a function of the density. We find that  $\Gamma_{\text{th}}$  becomes less sensitive to the density as  $T$  gets larger; e.g.,  $\Gamma_{\text{th}}$  is almost constant around  $\sim 1.4$  at  $T = 50$  MeV. The preceding *ab initio* calculation based on  $\chi$ EFT [69] is also overlaid on Fig. 6. Our  $\Gamma_{\text{th}}$  and the *ab initio*  $\Gamma_{\text{th}}$  [69] differ qualitatively; it may be partially because the slope of the *ab initio* EoS at  $T = 0$  is gentle compared with the state-of-the-art  $\chi$ EFT EoS [55, 56] to which our model is fitted to. We note that  $\Gamma_{\text{th}}$  in Fig. 6 is computed under the assumption of neutrinoless  $\beta$ -equilibrium. The values of  $\Gamma_{\text{th}}$

shown in this figure may deviate from effective values realized in dynamical astrophysical phenomena, particularly when neutrinos are trapped inside hot neutron stars.

## 5. Summary and outlooks

We demonstrated a successful construction of the equation of state based on the van der Waals prescription of the hadron resonance gas model with the Carnahan-Starling refinement of the excluded volume term. The ideal hadron resonance gas description does not work at high density as shown in Fig. 1; at  $T = 0$  both the repulsive and the attractive interactions are crucial. This statement itself is no surprise, but our proposal is that a very simple parametrization can fit in with the empirical EoSs. It is then a straightforward extension to include the finite- $T$  corrections. We quantified the thermal index,  $\Gamma_{\text{th}}$ , as a function of the density for various temperatures. Our estimated  $\Gamma_{\text{th}}$  favors a rather smaller value than the conventionally adopted one.

Our present modeling is the simplest one, and we can consider improvements in many respects. For example, the interaction should be species dependent, and in particular, the strangeness sector could behave differently. In some channels involving the strangeness, the Pauli blocking is relaxed and the short-range repulsive core is absent. As neutron stars contain hyperons as inevitable physical degrees of freedom, the flavor-dependent interactions should be considered along the line of Ref. [22]. It is also an interesting question to think of meson interaction effects. Moreover, since the validity region of our proposed model should cover the high- $T$  and low- $\mu_B$  regime, we can apply our predicted EoS for the heavy-ion collision experiments at lower collision energies. These await to be investigated as future extensions.

## Acknowledgments

YF thanks Koichi Murase for the consultation on numerical codes. The authors thank Koutarou Kyutoku, Koichi Murase, and Hiroyuki Tajima for useful discussions. This work was supported by Japan Society for the Promotion of Science (JSPS) KAKENHI Grant Nos. 18H01211, 19K21874, and 20J10506.

## References

- [1] S. Borsanyi, Z. Fodor, C. Hoelbling, S. D. Katz, S. Krieg, K. K. Szabo, Full result for the QCD equation of state with 2+1 flavors, *Phys. Lett. B* 730 (2014) 99–104. [arXiv:1309.5258](#), [doi:10.1016/j.physletb.2014.01.007](#).
- [2] A. Bazavov, et al., Equation of state in (2+1)-flavor QCD, *Phys. Rev. D* 90 (2014) 094503. [arXiv:1407.6387](#), [doi:10.1103/PhysRevD.90.094503](#).
- [3] A. Andronic, P. Braun-Munzinger, K. Redlich, J. Stachel, Decoding the phase structure of QCD via particle production at high energy, *Nature* 561 (7723) (2018) 321–330. [arXiv:1710.09425](#), [doi:10.1038/s41586-018-0491-6](#).
- [4] R. Hagedorn, J. Ranft, Statistical thermodynamics of strong interactions at high-energies. 2. Momentum spectra of particles produced in pp-collisions, *Nuovo Cim. Suppl.* 6 (1968) 169–354.
- [5] A. Monnai, B. Schenke, C. Shen, Equation of state at finite densities for QCD matter in nuclear collisions, *Phys. Rev. C* 100 (2) (2019) 024907. [arXiv:1902.05095](#), [doi:10.1103/PhysRevC.100.024907](#).
- [6] A. Bazavov, et al., Fluctuations and Correlations of net baryon number, electric charge, and strangeness: A comparison of lattice QCD results with the hadron resonance gas model, *Phys. Rev. D* 86 (2012) 034509. [arXiv:1203.0784](#), [doi:10.1103/PhysRevD.86.034509](#).
- [7] H. T. Ding, S. Mukherjee, H. Ohno, P. Petreczky, H. P. Schadler, Diagonal and off-diagonal quark number susceptibilities at high temperatures, *Phys. Rev. D* 92 (7) (2015) 074043. [arXiv:1507.06637](#), [doi:10.1103/PhysRevD.92.074043](#).
- [8] A. Bazavov, et al., The QCD Equation of State to  $\mathcal{O}(\mu_B^6)$  from Lattice QCD, *Phys. Rev. D* 95 (5) (2017) 054504. [arXiv:1701.04325](#), [doi:10.1103/PhysRevD.95.054504](#).
- [9] L. McLerran, R. D. Pisarski, Phases of cold, dense quarks at large  $N(c)$ , *Nucl. Phys. A* 796 (2007) 83–100. [arXiv:0706.2191](#), [doi:10.1016/j.nuclphysa.2007.08.013](#).
- [10] T. Kojo, Y. Hidaka, L. McLerran, R. D. Pisarski, Quarkyonic Chiral Spirals, *Nucl. Phys. A* 843 (2010) 37–58. [arXiv:0912.3800](#), [doi:10.1016/j.nuclphysa.2010.05.053](#).
- [11] T. Kojo, Y. Hidaka, K. Fukushima, L. D. McLerran, R. D. Pisarski, Interweaving Chiral Spirals, *Nucl. Phys. A* 875 (2012) 94–138. [arXiv:1107.2124](#), [doi:10.1016/j.nuclphysa.2011.11.007](#).
- [12] S. Lottini, G. Torrieri, Quarkyonic Percolation and deconfinement at finite density and number of colors, *Phys. Rev. C* 88 (2013) 024912. [arXiv:1204.3272](#), [doi:10.1103/PhysRevC.88.024912](#).
- [13] O. Philipsen, J. Scheunert, QCD in the heavy dense regime for general  $N_c$ : on the existence of quarkyonic matter, *JHEP* 11 (2019) 022. [arXiv:1908.03136](#), [doi:10.1007/JHEP11\(2019\)022](#).
- [14] A. Andronic, et al., Hadron Production in Ultra-relativistic Nuclear Collisions: Quarkyonic Matter and a Triple Point in the Phase Diagram of QCD, *Nucl. Phys. A* 837 (2010) 65–86. [arXiv:0911.4806](#), [doi:10.1016/j.nuclphysa.2010.02.005](#).
- [15] K. Fukushima, Hadron resonance gas and mean-field nuclear matter for baryon number fluctuations, *Phys. Rev. C* 91 (4) (2015) 044910. [arXiv:1409.0698](#), [doi:10.1103/PhysRevC.91.044910](#).
- [16] K. Fukushima, Y. Hidaka, Magnetic Shift of the Chemical Freeze-out and Electric Charge Fluctuations, *Phys. Rev. Lett.* 117 (10) (2016) 102301. [arXiv:1605.01912](#), [doi:10.1103/PhysRevLett.117.102301](#).
- [17] Y. Fujimoto, K. Fukushima, Y. Hidaka, Deconfining Phase Boundary of Rapidly Rotating Hot and Dense Matter and Analysis of Moment of Inertia, *Phys. Lett. B* 816 (2021) 136184. [arXiv:2101.09173](#), [doi:10.1016/j.physletb.2021.136184](#).
- [18] A. Andronic, P. Braun-Munzinger, J. Stachel, M. Winn, Interacting hadron resonance gas meets lattice QCD, *Phys. Lett. B* 718 (2012) 80–85. [arXiv:1201.0693](#), [doi:10.1016/j.physletb.2012.10.001](#).
- [19] D. H. Rischke, M. I. Gorenstein, H. Stoecker, W. Greiner, Excluded volume effect for the nuclear matter equation of state, *Z. Phys. C* 51 (1991) 485–490. [doi:10.1007/BF01548574](#).
- [20] R. Hagedorn, J. Rafelski, Hot Hadronic Matter and Nuclear Collisions, *Phys. Lett. B* 97 (1980) 136. [doi:10.1016/0370-2693\(80\)90566-3](#).
- [21] V. Vovchenko, M. I. Gorenstein, H. Stoecker, van der Waals Interactions in Hadron Resonance Gas: From Nuclear Matter to Lattice QCD, *Phys. Rev. Lett.* 118 (18) (2017) 182301. [arXiv:1609.03975](#), [doi:10.1103/PhysRevLett.118.182301](#).
- [22] V. Vovchenko, A. Motornenko, P. Alba, M. I. Gorenstein, L. M. Satarov, H. Stoecker, Multicomponent van der Waals equation of state: Applications in nuclear and hadronic physics, *Phys. Rev. C* 96 (4) (2017) 045202. [arXiv:1707.09215](#), [doi:10.1103/PhysRevC.96.045202](#).

- [23] V. Vovchenko, Hadron resonance gas with van der Waals interactions, *Int. J. Mod. Phys. E* 29 (05) (2020) 2040002. [arXiv:2004.06331](#), [doi:10.1142/S0218301320400029](#).
- [24] R. Hagedorn, Statistical thermodynamics of strong interactions at high-energies, *Nuovo Cim. Suppl.* 3 (1965) 147–186.
- [25] V. Vovchenko, D. V. Anchishkin, M. I. Gorenstein, Particle number fluctuations for the van der Waals equation of state, *J. Phys. A* 48 (30) (2015) 305001. [arXiv:1501.03785](#), [doi:10.1088/1751-8113/48/30/305001](#).
- [26] N. F. Carnahan, K. E. Starling, Equation of State for Nonattracting Rigid Spheres, *The Journal of Chemical Physics* 51 (2) (1969) 635–636. [doi:10.1063/1.1672048](#).
- [27] D. Anchishkin, V. Vovchenko, Mean-field approach in the multi-component gas of interacting particles applied to relativistic heavy-ion collisions, *J. Phys. G* 42 (10) (2015) 105102. [arXiv:1411.1444](#), [doi:10.1088/0954-3899/42/10/105102](#).
- [28] L. M. Satarov, K. A. Bugaev, I. N. Mishustin, Equation of state and sound velocity of a hadronic gas with a hard-core interaction, *Phys. Rev. C* 91 (5) (2015) 055203. [arXiv:1411.0959](#), [doi:10.1103/PhysRevC.91.055203](#).
- [29] L. M. Satarov, V. Vovchenko, P. Alba, M. I. Gorenstein, H. Stoecker, New scenarios for hard-core interactions in a hadron resonance gas, *Phys. Rev. C* 95 (2) (2017) 024902. [arXiv:1610.08753](#), [doi:10.1103/PhysRevC.95.024902](#).
- [30] O. Lourenço, M. Dutra, C. H. Lenzi, M. Bhuyan, S. K. Biswal, B. M. Santos, Density-dependent van der Waals model under the GW170817 constraint, *Astrophys. J.* 882 (2019) 67. [arXiv:1908.05114](#), [doi:10.3847/1538-4357/ab3122](#).
- [31] M. Dutra, B. M. Santos, O. Lourenço, Constraints and correlations of nuclear matter parameters from a density-dependent van der Waals model, *J. Phys. G* 47 (3) (2020) 035101. [arXiv:2002.02437](#), [doi:10.1088/1361-6471/ab5774](#).
- [32] A. Bauswein, H. T. Janka, R. Oechslin, Testing Approximations of Thermal Effects in Neutron Star Merger Simulations, *Phys. Rev. D* 82 (2010) 084043. [arXiv:1006.3315](#), [doi:10.1103/PhysRevD.82.084043](#).
- [33] A. Figura, J. J. Lu, G. F. Burgio, Z. H. Li, H. J. Schulze, Hybrid equation of state approach in binary neutron-star merger simulations, *Phys. Rev. D* 102 (4) (2020) 043006. [arXiv:2005.08691](#), [doi:10.1103/PhysRevD.102.043006](#).
- [34] B. Fore, S. Reddy, Pions in hot dense matter and their astrophysical implications, *Phys. Rev. C* 101 (3) (2020) 035809. [arXiv:1911.02632](#), [doi:10.1103/PhysRevC.101.035809](#).
- [35] G. Torrieri, I. Mishustin, The nuclear liquid-gas phase transition at large  $N_c$  in the Van der Waals approximation, *Phys. Rev. C* 82 (2010) 055202. [arXiv:1006.2471](#), [doi:10.1103/PhysRevC.82.055202](#).
- [36] K. Masuda, T. Hatsuda, T. Takatsuka, Hadron-Quark Crossover and Massive Hybrid Stars with Strangeness, *Astrophys. J.* 764 (2013) 12. [arXiv:1205.3621](#), [doi:10.1088/0004-637X/764/1/12](#).
- [37] G. Baym, S. Furusawa, T. Hatsuda, T. Kojo, H. Togashi, New Neutron Star Equation of State with Quark-Hadron Crossover, *Astrophys. J.* 885 (2019) 42. [arXiv:1903.08963](#), [doi:10.3847/1538-4357/ab441e](#).
- [38] Y. Fujimoto, K. Fukushima, W. Weise, Continuity from neutron matter to two-flavor quark matter with  $^1S_0$  and  $^3P_2$  superfluidity, *Phys. Rev. D* 101 (9) (2020) 094009. [arXiv:1908.09360](#), [doi:10.1103/PhysRevD.101.094009](#).
- [39] K. Fukushima, T. Kojo, The Quarkyonic Star, *Astrophys. J.* 817 (2) (2016) 180. [arXiv:1509.00356](#), [doi:10.3847/0004-637X/817/2/180](#).
- [40] L. McLerran, S. Reddy, Quarkyonic Matter and Neutron Stars, *Phys. Rev. Lett.* 122 (12) (2019) 122701. [arXiv:1811.12503](#), [doi:10.1103/PhysRevLett.122.122701](#).
- [41] K. S. Jeong, L. McLerran, S. Sen, Dynamically generated momentum space shell structure of quarkyonic matter via an excluded volume model, *Phys. Rev. C* 101 (3) (2020) 035201. [arXiv:1908.04799](#), [doi:10.1103/PhysRevC.101.035201](#).
- [42] S. Sen, N. C. Warrington, Finite-temperature quarkyonic matter with an excluded volume model, *Nucl. Phys. A* 1006 (2021) 122059. [arXiv:2002.11133](#), [doi:10.1016/j.nuclphysa.2020.122059](#).
- [43] D. C. Duarte, S. Hernandez-Ortiz, K. S. Jeong, Excluded-volume model for quarkyonic Matter: Three-flavor baryon-quark Mixture, *Phys. Rev. C* 102 (2) (2020) 025203. [arXiv:2003.02362](#), [doi:10.1103/PhysRevC.102.025203](#).
- [44] D. C. Duarte, S. Hernandez-Ortiz, K. S. Jeong, Excluded-volume model for quarkyonic matter. II. Three-flavor shell-like distribution of baryons in phase space, *Phys. Rev. C* 102 (6) (2020) 065202. [arXiv:2007.08098](#), [doi:10.1103/PhysRevC.102.065202](#).
- [45] T. Zhao, J. M. Lattimer, Quarkyonic Matter Equation of State in Beta-Equilibrium, *Phys. Rev. D* 102 (2) (2020) 023021. [arXiv:2004.08293](#), [doi:10.1103/PhysRevD.102.023021](#).
- [46] G. Cao, J. Liao, A field theoretical model for quarkyonic matter, *JHEP* 10 (2020) 168. [arXiv:2007.02028](#), [doi:10.1007/JHEP10\(2020\)168](#).
- [47] K. Fukushima, T. Kojo, W. Weise, Hard-core deconfinement and soft-surface delocalization from nuclear to quark matter, *Phys. Rev. D* 102 (9) (2020) 096017. [arXiv:2008.08436](#), [doi:10.1103/PhysRevD.102.096017](#).
- [48] P. M. Lo, B. Friman, K. Redlich, C. Sasaki, S-matrix analysis of the baryon electric charge correlation, *Phys. Lett. B* 778 (2018) 454–458. [arXiv:1710.02711](#), [doi:10.1016/j.physletb.2018.01.016](#).
- [49] S. Wheaton, J. Cleymans, THERMUS: A Thermal model package for ROOT, *Comput. Phys. Commun.* 180 (2009) 84–106. [arXiv:hep-ph/0407174](#), [doi:10.1016/j.cpc.2008.08.001](#).
- [50] V. Vovchenko, D. V. Anchishkin, M. I. Gorenstein, Van der Waals Equation of State with Fermi Statistics for Nuclear Matter, *Phys. Rev. C* 91 (6) (2015) 064314. [arXiv:1504.01363](#), [doi:10.1103/PhysRevC.91.064314](#).
- [51] K. Redlich, K. Zalewski, Thermodynamics of Van der Waals Fluids with quantum statistics, *Acta Phys. Polon. B* 47 (2016) 1943. [arXiv:1605.09686](#), [doi:10.5506/APhysPolB.47.1943](#).
- [52] V. Vovchenko, Equations of state for real gases on the nuclear scale, *Phys. Rev. C* 96 (1) (2017) 015206. [arXiv:1701.06524](#), [doi:10.1103/PhysRevC.96.015206](#).
- [53] N. Ishii, S. Aoki, T. Hatsuda, The Nuclear Force from Lattice QCD, *Phys. Rev. Lett.* 99 (2007) 022001. [arXiv:nucl-th/0611096](#), [doi:10.1103/PhysRevLett.99.022001](#).
- [54] F. Douchin, P. Haensel, A unified equation of state of dense matter and neutron star structure, *Astron. Astrophys.* 380 (2001) 151. [arXiv:astro-ph/0111092](#), [doi:10.1051/0004-6361:20011402](#).
- [55] C. Drischler, S. Han, J. M. Lattimer, M. Prakash, S. Reddy, T. Zhao, Limiting masses and radii of neutron stars and their implications, *Phys. Rev. C* 103 (4) (2021) 045808. [arXiv:2009.06441](#), [doi:10.1103/PhysRevC.103.045808](#).
- [56] C. Drischler, R. J. Furnstahl, J. A. Melendez, D. R. Phillips, How Well Do We Know the Neutron-Matter Equation of State at the Densities Inside Neutron Stars? A Bayesian Approach with Correlated Uncertainties, *Phys. Rev. Lett.* 125 (20) (2020) 202702. [arXiv:2004.07232](#), [doi:10.1103/PhysRevLett.125.202702](#).
- [57] T. E. Riley, et al., A *NICER* View of PSR J0030+0451: Millisecond Pulsar Parameter Estimation, *Astrophys. J. Lett.* 887 (1) (2019) L21. [arXiv:1912.05702](#), [doi:10.3847/2041-8213/ab481c](#).
- [58] M. C. Miller, et al., PSR J0030+0451 Mass and Radius from *NICER* Data and Implications for the Properties of Neutron Star Matter, *Astrophys. J. Lett.* 887 (1) (2019) L24. [arXiv:1912.05705](#), [doi:10.3847/2041-8213/ab50c5](#).
- [59] T. E. Riley, et al., A *NICER* View of the Massive Pulsar PSR J0740+6620 Informed by Radio Timing and XMM-Newton Spectroscopy (5 2021). [arXiv:2105.06980](#).
- [60] M. C. Miller, et al., The Radius of PSR J0740+6620 from *NICER* and XMM-Newton Data (5 2021). [arXiv:2105.06979](#).
- [61] S. Weinberg, *Gravitation and Cosmology: Principles and Applications of the General Theory of Relativity*, John Wiley and Sons, New York, 1972.

- [62] B. Margalit, B. D. Metzger, Constraining the Maximum Mass of Neutron Stars From Multi-Messenger Observations of GW170817, *Astrophys. J. Lett.* 850 (2) (2017) L19. [arXiv:1710.05938](#), [doi:10.3847/2041-8213/aa991c](#).
- [63] M. Shibata, S. Fujibayashi, K. Hotokezaka, K. Kiuchi, K. Kyutoku, Y. Sekiguchi, M. Tanaka, Modeling GW170817 based on numerical relativity and its implications, *Phys. Rev. D* 96 (12) (2017) 123012. [arXiv:1710.07579](#), [doi:10.1103/PhysRevD.96.123012](#).
- [64] L. Rezzolla, E. R. Most, L. R. Weih, Using gravitational-wave observations and quasi-universal relations to constrain the maximum mass of neutron stars, *Astrophys. J. Lett.* 852 (2) (2018) L25. [arXiv:1711.00314](#), [doi:10.3847/2041-8213/aaa401](#).
- [65] M. Ruiz, S. L. Shapiro, A. Tsokaros, GW170817, General Relativistic Magnetohydrodynamic Simulations, and the Neutron Star Maximum Mass, *Phys. Rev. D* 97 (2) (2018) 021501. [arXiv:1711.00473](#), [doi:10.1103/PhysRevD.97.021501](#).
- [66] E. Annala, T. Gorda, A. Kurkela, J. Nättilä, A. Vuorinen, Evidence for quark-matter cores in massive neutron stars, *Nature Phys.* 16 (9) (2020) 907–910. [arXiv:1903.09121](#), [doi:10.1038/s41567-020-0914-9](#).
- [67] Y. Fujimoto, K. Fukushima, Equation of state of cold and dense QCD matter in resummed perturbation theory (11 2020). [arXiv:2011.10891](#).
- [68] G. F. Burgio, I. Vidana, H. J. Schulze, J. B. Wei, Neutron stars and the nuclear equation of state, *Prog. Part. Nucl. Phys.* 120 (2021) 103879. [arXiv:2105.03747](#), [doi:10.1016/j.pnpnp.2021.103879](#).
- [69] A. Carbone, A. Schwenk, Ab initio constraints on thermal effects of the nuclear equation of state, *Phys. Rev. C* 100 (2) (2019) 025805. [arXiv:1904.00924](#), [doi:10.1103/PhysRevC.100.025805](#).
- [70] H. T. Janka, T. Zwerger, R. Moenchmeyer, Does artificial viscosity destroy prompt type-II supernova explosions?, *Astron. Astrophys.* 268 (1) (1993) 360–368.
- [71] K. Hotokezaka, K. Kiuchi, K. Kyutoku, T. Muranushi, Y.-i. Sekiguchi, M. Shibata, K. Taniguchi, Remnant massive neutron stars of binary neutron star mergers: Evolution process and gravitational waveform, *Phys. Rev. D* 88 (2013) 044026. [arXiv:1307.5888](#), [doi:10.1103/PhysRevD.88.044026](#).
- [72] H. Yasin, S. Schäfer, A. Arcones, A. Schwenk, Equation of state effects in core-collapse supernovae, *Phys. Rev. Lett.* 124 (9) (2020) 092701. [arXiv:1812.02002](#), [doi:10.1103/PhysRevLett.124.092701](#).